Journal of Luminescence 199 (2018) 372–378

Contents lists available at ScienceDirect

Journal of Luminescence

journal homepage: www.elsevier.com/locate/jlumin

Energy transfer between terbium and europium ions in barium orthosilicate phosphors obtained from sol-gel route

Airton G. Bispo-Jr[a,b], Sergio A.M. Lima[a,b], Ana. M. Pires[a,b,*]

[a] São Paulo State University (Unesp), School of Technology and Sciences, Presidente Prudente, SP 19060-900, Brazil
[b] São Paulo State University (Unesp), Institute of Biosciences, Humanities and Exact Sciences, São José do Rio Preto, SP 15054-000, Brazil

ARTICLE INFO

Keywords:
Silicate
Europium
Terbium
Energy transfer
Van Uitert theory
Spectroscopic probe

ABSTRACT

The present paper reports on the energy transfer mechanism between Eu^{3+} and Tb^{3+} in barium orthosilicate obtained from the sol-gel route, when both activators concentration is varied. The synthetic methodology was adjusted to provide high crystalline and monophasic Ba_2SiO_4. In the emission spectra under 250 nm excitation, both Eu^{3+} ($^5D_0 \rightarrow {}^7F_J$) and Tb^{3+} ($^5D_3 \rightarrow {}^7F_J$ and $^5D_4 \rightarrow {}^7F_J$) transitions can be observed at low Eu^{3+} doping concentrations with an unexpected and intense blue emission from Tb^{3+}. However, when the Eu^{3+} content is higher than that of the Tb^{3+}, just the Eu^{3+} emission is noticed. Also, it is possible to tune the phosphor emission from red to pink by varying the Eu^{3+} and Tb^{3+} content. From the excitation spectra, we inferred that energy transfer (ET) from Tb^{3+} to Eu^{3+} occurs at any doping situation, nonetheless, the opposite process happens just when both activators amount is similar. An approach using the Tb^{3+} and Eu^{3+} lifetimes and the Eu^{3+} quantum efficiency confirms this observation, indicating that not only the matrix act as sensitizer to the Eu^{3+} ions, but also Tb^{3+} ions contribute by increasing the Eu^{3+} quantum efficiency in up to 20%. Finally, by using the Van Uitert theory, it was found for this system that the ET between the two rare-earth ions is dominated by the dipole-dipole mechanism.

1. Introduction

Rare earth (RE)-doped nanophosphors display unique optical properties that combined with good thermal and chemical stability, make these systems suitable for luminescence and photonic applications [1]. In special, RE-doped barium orthosilicate have been used in solid state lighting devices as white light emitting diode (w-LEDs) [2,3] which are replacing fluorescent and incandescent light sources due to their high energy conversion efficiency resulting in an energy saving, compactness, and long duration time [4,5]. Eu^{3+} ion, for instance, is an efficient red emitting activator due to its emission lines that arise from the $^5D_0$ excited level to the ^7F_J (J = 0, 1, 2, 3, 4, 5, 6) ground levels [6,7]. Also, the relative intensity, position and degenerescence of Eu^{3+} transitions are dependent on the host lattice nature, chemical composition and crystalline structure, allowing its use as structural probes [8]. Tb^{3+}, in turn, has two main emission levels $^5D_4$, and $^5D_3$ [9]. The transitions from the first one to the ground ^7F_J levels result in green emission, while the transitions from the second one is less common, resulting in blue emission, and depend on the Tb^{3+} concentration, and on the crystal structure and phonon frequency of the matrix [10]. Ba_2SiO_4 is an inorganic insulator matrix widely used to host RE activators due its relative low phonon frequency (~900 cm^{-1}) and high structural, thermal and electrical stability [11,12]. For the best of your knowledge, no study has been reported about the synthesis of barium orthosilicate simultaneously doped with Eu^{3+} and Tb^{3+}, while recently, we reported the synthesis of the Eu^{3+}-doped Ba_2SiO_4 from the sol gel-route [13]. On the other side, many reports on the synthesis of Eu^{3+} and Tb^{3+}-codoped phosphors based on host lattices distinct from Ba_2SiO_4 can be found in the literature, aiming application in white LEDs devices [14–18]. As example, M. A. Tshabalala et al. [19] described the solid state synthesis of Eu^{3+} and Tb^{3+}-doped strontium orthosilicate and its white emission under UV excitation. However, one of the challenges concerning these codoped phosphors is to understand the energy transfer (ET) mechanism between Eu^{3+} and Tb^{3+} ions in order to modulate the phosphor white emission. Indeed, there is a lack in the literature about this kind of approach dealing with ET between these ions specifically in barium orthosilicate matrix. In this paper, we report the synthesis of Eu^{3+} and Tb^{3+}-codoped barium orthosilicate phosphor from the sol-gel route, and we propound a detailed interpretation of the ET process by varying the concentration of the two activator ions in order to use Tb^{3+}, along with the matrix, as sensitizer for the Eu^{3+} emission.

* Corresponding author at: São Paulo State University (Unesp), School of Technology and Sciences, R. Roberto Simonsen, 305, 19060-900 Presidente Prudente, SP, Brazil.
E-mail address: ana.maria@unesp.br (A.M. Pires).

https://doi.org/10.1016/j.jlumin.2018.03.057
Received 30 November 2017; Received in revised form 17 March 2018; Accepted 20 March 2018
Available online 24 March 2018

2. Experimental

The Tb^{3+} and Eu^{3+}-codoped Ba_2SiO_4 powder samples were synthesized by applying an adapted sol-gel route developed in our research group [13,20]. Tetraethylorthosilicate (TEOS, $C_8H_{20}O_4Si$, 99.9%, Fluka), hydrogen peroxide (H_2O_2, 36%, Synth), acetic acid (CH_3COOH, 97%, VETEC), barium acetate ($Ba(CH_3COO)_2$, 99.9%, VETEC), europium oxide (Eu_2O_3, 99.99%, Aldrich), hydrochloric acid (HCl, 37%, Sigma), and terbium oxide (Tb_4O_7, 99.99%, Aldrich) were used as reactants. Europium acetate ($Eu(CH_3COO)_3$) and terbium chloride ($TbCl_3$) solutions were prepared by dissolving the RE oxide in hot acetic acid or hydrochloric acid, respectively. For the complete dissolution of the Tb_4O_7, it was necessary the addition of some drops of H_2O_2. The xerogel precursors for the Ba_2SiO_4 powders were synthesized by dissolving stoichiometric amount of $Ba(CH_3COO)_2$, $Eu(CH_3COO)_3$ and $TbCl_3$ in acetic acid (10 mL), aiming to obtain 1.0000 g of $Ba_xEu_yTb_zSiO_4$ powder. Following, TEOS (0.55 M, in isopropyl alcohol) was stoichiometrically added in the solution containing the metal precursors. The solution was kept under magnetic stirring for 4 h (35 °C) until the gel precursor formation. The gel was dried at 120 °C for 2 h, resulting in the xerogel phase. Finally, the xerogel precursor was calcinated at 1100 °C for 2 h with a heating ramp of 10 °C/min in an EDG muffle furnace type, under a circulating air atmosphere, obtaining the phosphor particles. The Eu^{3+} and Tb^{3+} amounts were isoelectronically varied in order to keep the same overall charge in the system, according to the Ba^{2+}, Eu^{3+}, Tb^{3+} and SiO_4^{4-} charges ($3n_{Eu^{3+}} + 3n_{Tb^{3+}} + 2n_{Ba^{2+}} = +4$, where $n_{Ba^{2+}}$, $n_{Tb^{3+}}$ and $n_{Eu^{3+}}$ are the mol number of Ba^{2+}, Tb^{3+} and Eu^{3+}, respectively). The stoichiometric amounts of Eu^{3+}, Tb^{3+} and Ba^{2+} ions in each phosphor are shown in the Supplementary material, Table ES1, and the samples synthesized are listed in Table 1.

Powder crystalline structure was checked by using a SIEMENS diffractometer model D5000, Cu Kα radiation (λ = 1,5405 Å), a 2θ range of 20–45°, an increment of 0.02° and integration time of 1 s. The samples were also characterized by scanning electron microscopy (SEM) using a Carls Zeiss model EVO LS15 microscope with a detector of secondary electrons (SE) in high vacuum and constant temperature. Finally, photoluminescence measurements at room temperature were carried out in a Horiba JobinYvon spectrometer Fluorolog-3 with a Xe lamp (450 W) source with double excitation monochromator. Emission lifetime was evaluated using a phosphorimeter equipped with Xe (5 J/pulse) lamp.

Table 1
Tb/Eu emission rate, and critical distance (R_c) between Eu^{3+} and Tb^{3+} ions.

Tb/ Eu (%)	Tb/Eu emission rate[a]	R_c Eu-Eu/ Å[b]	R_c Tb-Tb / Å[b]	R_c Eu-Tb / Å[b]
2/2	1.19	8.54	8.54	6.78
2/0.1	0.09	23.5	8.62	8.49
1/3	–	7.46	10.8	6.78
1/2	0.58	8.58	10.8	7.50
1/1	0.92	8.67	10.9	8.63
1/0.1	0.48	23.5	10.9	10.6
1/0.05	0.59	29.7	10.9	10.7
1/0.01	0.34	50.7	10.9	10.9
0.5/4	–	6.76	13.5	6.50
0.5/1	1.13	10.90	13.7	9.52
0.5/0.5	0.96	13.7	13.7	10.9
0.1/4	–	6.77	23.2	10.4

[a] The Tb/Eu emission rate parameter was determined by the rate between the sum of the integrated area below the Terbium and Europium transitions in the emission spectra under excitation at 250 nm.

[b] The Ln-Ln distance was calculated considering the Ln^{3+} concentration in Eq. (2).

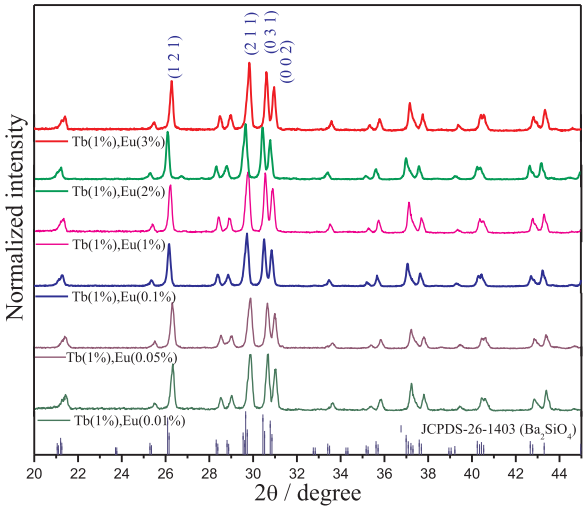

Fig. 1. Powder X-ray diffractograms of the phosphors doped with 1% of Tb^{3+} and varying the Eu^{3+} content.

3. Results

X-ray diffraction (XRD) patterns of representative samples are shown in Fig. 1 and for all other samples, the results are shown in Fig. S1, Supplementary material. XRD data confirm that the phosphors obtained by the sol-gel route at 1100 °C are crystalline, with orthorhombic crystal system (JCPDS 26–1403 card), and P_{man} space group. Regarding the limit of detection of this technique, there is no evidence of Eu_2O_3 and Tb_4O_7 formation, which corroborate for the fact that both activator ions are inserted into the Ba_2SiO_4 lattice and can occupy two different sites, one with coordination number (CN) 9 and another with CN 10 [21]. In addition, the mean crystallite size calculated via Scherrer's method [22], varied from 49 to 76 nm for all produced samples. The full data are included in the Supplementary material, Table ES2. Moreover, it is clear that the increase of the Eu^{3+} concentration in relation to the Tb^{3+} leads to an increase in the mean diameter of the crystallites.

SEM images of some representative phosphors are shown in Fig. S2, in the Supplementary material. The observed particles are irregular in shape and size, yet the mean size was estimated at about 330 nm, and some particles are spherical while others are ellipsoidal shaped.

Fig. 2 exhibits the photoluminescence excitation spectra of the co-doped phosphors monitoring the $^5D_0 \rightarrow {}^7F_2$ transition of Eu^{3+} at 612 nm. The most intense band observed in the excitation spectra at high energies is assigned to both Tb^{3+} $^7F_6 \rightarrow 4f^7 5d$ transition and $O^{2-} \rightarrow Eu^{3+}$ charge transfer. The magnification of the range within 325–500 nm shows the Eu^{3+} and the Tb^{3+} *f-f* transitions in all spectra, indicating that the Eu^{3+} emission arises from both RE^{3+} excitation. This observation lead us to conclude that the ET from Tb^{3+} to Eu^{3+} ions ($Tb^{3+} \rightarrow Eu^{3+}$) is taking place in all phosphors. The ET between the two ions is favored because the energies of the $^5D_3$ (26,402 cm^{-1}) and $^5D_4$ (20,640 cm^{-1}) [23] levels of Tb^{3+} ions, and the $^5D_0$ (17,280 cm^{-1}), $^5D_1$ (18,973 cm^{-1}), $^5D_2$ (21,445 cm^{-1}), and $^5D_3$ (24,335) [6] levels of Eu^{3+} ions are close enough to allow the resonance between them.

In the emission spectra recorded with excitation wavelength fixed at 250 nm, Fig. 3, both ions are excited via Tb^{3+} $^7F_6 \rightarrow 4f^7 5d$ and $O^{2-} \rightarrow Eu^{3+}$ transitions, resulting in green and blue emission from Tb^{3+}, and red emission from Eu^{3+}. When the Eu^{3+} content is much higher than that of Tb^{3+}, the Tb^{3+} emission is neglected, just the matrix intrinsic emission is observed in the blue range (see the matrix intrinsic luminescent profile in Fig. S4).

The Eu^{3+} red emission comes from the $^5D_0 \rightarrow {}^7F_{0,1,2,3,4}$ transitions, attributed to Eu^{3+} ions occupying low-symmetry sites [24]. The Tb^{3+}

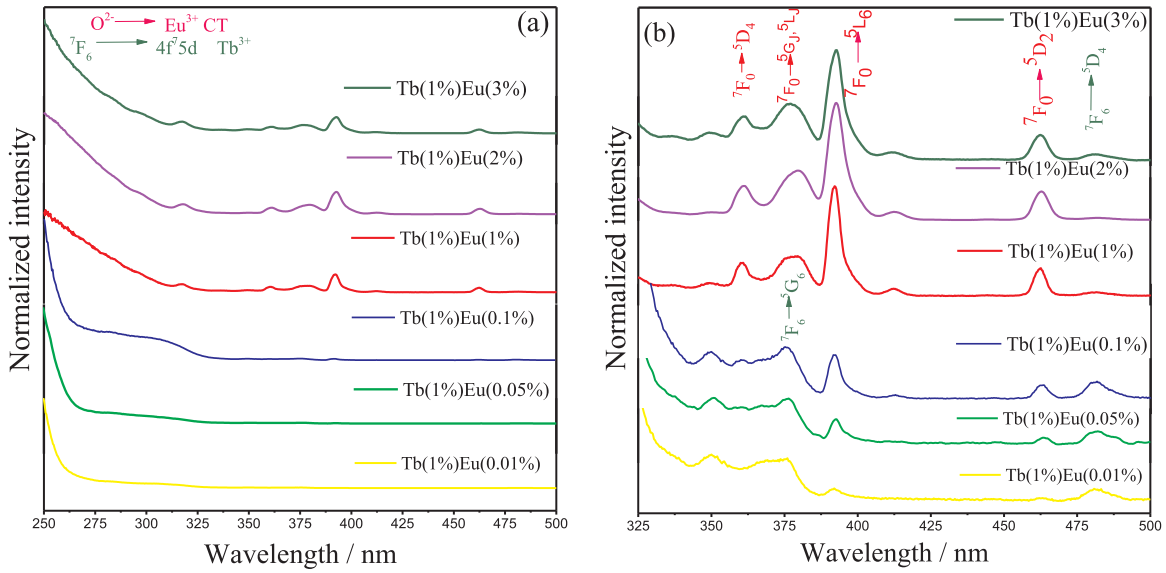

Fig. 2. Excitation spectra of Ba_2SiO_4:Tb^{3+},Eu^{3+} samples measured at room temperature. The emission wavelength was fixed in the Eu^{3+} emission at 612 nm **(a).** Magnification of the range between 325 and 500 nm, where Tb^{3+} transitions assignments are shown in green and the Eu^{3+} ones in red **(b).** The excitation spectra of the other phosphors are shown in Fig. ES3.

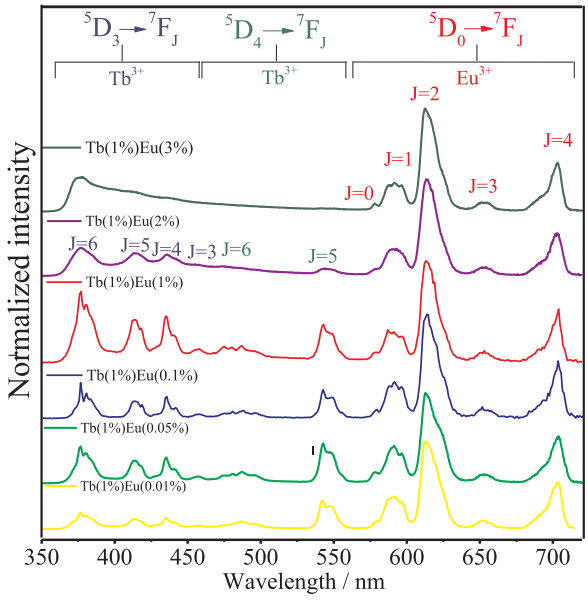

Fig. 3. Emission spectra of Ba_2SiO_4:Tb^{3+},Eu^{3+} samples measured at room temperature. The emission spectra of the other phosphors are shown in Fig. S5. The excitation wavelength was fixed in 250 nm. Tb^{3+} transitions assignments are shown in green and blue and Eu^{3+} in red.

blue emission, in turn, is assigned to transitions from the $^5D_3$ excited level while the green emission comes from the $^5D_4$ level to the ^7F_J ground level. Usually, the Tb^{3+} blue emission is very weak due to the cross relaxation mechanism involving the $^5D_3$ and $^5D_4$ levels which quenches the $^5D_3$ emission (see Eq. (1)) [25]. However, when the Tb^{3+} concentration is low, the Tb-Tb distance is long enough to inhibit the cross relaxation, favoring the blue emission from the $^5D_3$ level. In literature, the Tb^{3+} blue emission is reported for concentration less than 0.01 at% [10,25], but in the present case, the intense blue emission begins to take place at Tb^{3+} concentrations relatively high (~1%). Also, host matrix with phonon energy lower than 1000 cm^{-1} favors the $^5D_3$ blue emission due to the absence of multi phonon relaxation [26]. The phonon energy in the barium orthosilicate is 900 cm^{-1} [26], then the multiphonon relaxation process that can compete with the $^5D_3$ radiative emission is unlikely to take place, since the multiphonon mechanism is limited by the coupling of a maximum of 4 or 5 phonons [26].

$$Tb^{3+}(^5D_3)+Tb^{3+}(^7F_6)\rightarrow Tb^{3+}(^5D_4)+Tb^{3+}(^7F_0) \quad (1)$$

The rate between terbium and europium emission integrated areas for all phosphors is listed in Table 1. For the samples doped with 1% of Tb^{3+}, the increase of Eu^{3+} concentration leads to an increment in the Tb^{3+} emission up to 1% of Eu^{3+}. Then, the Eu^{3+} emission overcomes the Tb^{3+} one. This behavior leads us to conclude that ET from Eu^{3+} to Tb^{3+} ($Eu^{3+}\rightarrow Tb^{3+}$) dominates the ET up to 1% of Eu^{3+}, and at higher Eu^{3+} concentrations, on the other side, the $Tb^{3+}\rightarrow Eu^{3+}$ ET is the main process. The same profile is observed for samples doped with 0.5% of Tb^{3+}.

The $Eu^{3+}\rightarrow Tb^{3+}$ ET mechanism proposition is indorsed by analyzing the excitation spectra monitoring the Tb^{3+} $^5D_4\rightarrow{}^7F_5$ emission (Fig. S6), where the Eu^{3+} $^7F_0\rightarrow{}^5L_6$ transition is observed for the sample doped with 1% of Eu^{3+} and Tb^{3+}, indicating that Tb^{3+} emission can be achieved via Eu^{3+} excitation. For the samples with low Eu^{3+} concentrations, the Eu^{3+} excitation cannot be observed because the Ba_2SiO_4 intrinsic excitation overcomes the Tb^{3+} lines.

An extrapolation of Eu^{3+}-doping in relation to the Tb^{3+} concentration (sample doped with 0.1% of Tb^{3+} and 4% of Eu^{3+}) shows that the Tb^{3+} emission is quenched when the Eu^{3+} content is too high. In addition, when both Eu^{3+} and Tb^{3+} doping are the same, the Tb^{3+} and Eu^{3+} emission intensity are similar, probably because the $Eu^{3+}\rightarrow Tb^{3+}$ and $Tb^{3+}\rightarrow Eu^{3+}$ ET rates are too close in these cases. Therefore, the Eu→Tb ET occurs just when both the Eu^{3+} and Tb^{3+} content are close.

Fig. 4 shows some propositions of ET mechanisms between Tb^{3+} and Eu^{3+} in Ba_2SiO_4 host. In the mechanism I, both Eu^{3+} and Tb^{3+} emit under 250 nm excitation. In the mechanism II, the ET from Tb^{3+} to Eu^{3+} is shown and occurs for all samples, dominating the ET profile at high Eu^{3+} concentrations. In the case of mechanism III, the ET from Eu^{3+} to Tb^{3+} is represented and dominate the ET between the RE ions just for samples with low Eu^{3+} doping concentrations.

Usually, the energy transfer among RE ions involves radiation reabsorption, exchange or multipole–multipole interactions [27]. However, in the present system, the radiation reabsorption mechanism is unlikely to take place because it requires a wide overlap between the donor emission and acceptor excitation spectra, which is not observed

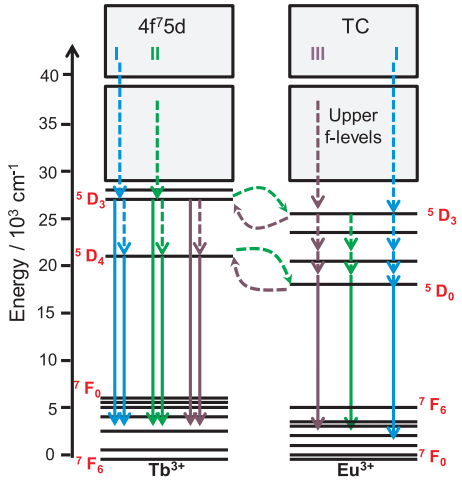

Fig. 4. Energy transfer mechanisms between Tb^{3+} and Eu^{3+} ions (dashed arrows: non-radiative transitions; solid line arrows: radiative transitions, curved lines: energy transfer). The mechanism I (blue lines) represent the emission from both RE ions under excitation at 250 nm without energy transfer. The mechanism II (green lines) represent the $Tb^{3+}\rightarrow Eu^{3+}$ ET and the emission from both RE ions. The mechanism III (purple lines) represent the $Eu^{3+}\rightarrow Tb^{3+}$ ET and both RE emissions. (For interpretation of the references to color in this figure legend, the reader is referred to the web version of this article.)

in this system. Considering the exchange coupling possibility, it is necessary to evaluate the critical distance (R_c) between the donor and acceptor because this mechanism is limited by 4 Å to allow an orbital overlap [28]. In this context, the critical distance was determinate by using Eq. (2) [29], where n_A is equal to $(x.n)/V$, V is the unit cell volume (V = 444.257 Å, from the JCPDS-26–1403 card), x is the dopant concentration, and n is the Ba^{2+} mol number per unit cell (n = 8 from the JCPDS-26–1403 card). The estimated critical distance is shown in Table 1.

$$R_c = \left[\frac{3}{4\pi n_A}\right]^{1/3} \tag{2}$$

The calculated R_C indicates that an exchange interaction is unlikely to take place since the values are higher than 4 Å. Thus, the multipolar interaction must be the main factor that contributes to the energy transfer mechanism.

In order to investigate the dominant multipolar mechanism responsible for the ET between Eu^{3+} and Tb^{3+} ions, it was used the theoretical model developed by Van Uitert [30] showed in the Eq. (3), where x is the acceptor concentration, I is the emission intensity obtained from the emission spectra, and β is a constant. In this model, θ is a function of the dominant ET mechanism between the donor and acceptor species. Electric dipole–dipole (D–D) interactions are represented by θ = 6, electric dipole–quadrupole (D–Q) interactions correspond to θ = 8 and electric quadrupole–quadrupole (Q–Q) interactions, in turn, are represented by θ = 10. In Fig. 5 it is plotted the log (x) versus log(I/x), where the intensity was fixed in both Tb^{3+} $^5D_4\rightarrow{}^7F_5$ and Eu^{3+} $^5D_0\rightarrow{}^7F_2$ transitions. The θ values deduced from the fitting plots monitoring the emission of both RE ions are closer to 6, suggesting that D–D interaction are the main contribution for the ET between Tb^{3+} and Eu^{3+} ions in the Ba_2SiO_4 matrix.

$$\frac{I}{x} = [1+\beta(x)^{\theta/3}]^{-1} \tag{3}$$

The CIE chromaticity coordinates obtained for all phosphors are presented in the diagram in Fig. 6. When the Tb^{3+} concentration is fixed at 1%, the emission moves to pink, when the Eu^{3+} concentration increase from 0.01 up to 1%, then goes back to red. This occurs because the Tb^{3+} emission is favored up to 1% of Eu^{3+}, from then on, the Eu^{3+} emission overcomes the Tb^{3+} emission. Samples with equal RE concentration emit near to pink, since both red and blue emissions of Eu^{3+} and Tb^{3+} respectively have similar intensities. The phosphors with low Tb^{3+} concentration emit near to pink due to the blue contribution of the matrix emission. Thus, the emission color is tunable by varying the dopant concentration.

The Judd-Ofelt intensity parameters were evaluated from the emission spectra data and its values are summarized in Table 2. In this theory, the $^5D_0\rightarrow{}^7F_2$ and $^5D_0\rightarrow{}^7F_4$ transitions are directly correlated to Ω_2 and Ω_4 intensity parameters, which can be calculated from the integrated areas below the transitions $^5D_0\rightarrow{}^7F_1$, $^5D_0\rightarrow{}^7F_2$, and $^5D_0\rightarrow{}^7F_4$, as shown in Eqs. (4) and (5) [32].

$$A_{0-\lambda} = A_{0-j} = A_{01}\frac{I_{0-j}}{I_{0-1}}\frac{h\nu_{0-1}}{h\nu_{0-j}} \tag{4}$$

$$\sum_{\lambda=2,4}\Omega_\lambda\langle{}^5D_0\rangle^2 = A_{01}\frac{I_{0-j}}{I_{0-1}}\frac{h\nu_{0-1}}{h\nu_{0-j}}\frac{3hc^3 4\epsilon_0}{64\pi^3 e^2}\frac{1}{\nu_\lambda{}^3 x} \tag{5}$$

Where the term $\langle{}^5D_0\rangle^2$ represent the square reduced matrix elements which is equal to 0.0032 and 0.0023 for Ω_2 and Ω_4; respectively [32]; e, h, ε_0 and c are the electron charge, the Planck's constant, the vacuum permittivity constant; and the speed of light in vacuum, respectively; A_{01} is equal to 14.65.n [3] (n is the refractive index considered in this case as 1.7 [13]) and corresponds to the Einstein's coefficient for spontaneous emission [33]; $I_{0\text{-}j}$ is the integrated area under the respective $^5D_0\rightarrow{}^7F_j$ transitions; and x is given by $n(n^2+2)^2/9$ and corresponds to the Lorentz local field correction.

The relatively low values of Ω_4 compared to other systems [34,35] indicate that the chemical environment around Eu^{3+} is low polarizable, suggesting a low covalence degree of the Eu-O bond, since the Ω_4 intensity parameter is more sensitive to changes in the electron density around the Eu^{3+}, caused by variations in the Eu-O bond distance [36]. On the other hand, the Ω_2 value is more sensitive to changes in the Eu^{3+} site symmetry related to angular distortions in the Eu-O bonds [37]. The relatively low values of Ω_2 intensity parameters compared to other systems [34,35] indicate that the environment around the Eu^{3+} ions is relatively symmetric. This occurs because the doping does not cause strong distortions in the Eu^{3+} sites [13]. Also, there is a tendency of enhancement for the Ω_2 values when the Eu^{3+} concentration increase, showing that the Eu^{3+} local symmetry is lowered. The $^5D_0\rightarrow{}^7F_2$ is considered hypersensitive to the environment, and its intensity increase as the symmetry around the Eu^{3+} ion decrease.

Emission lifetime (τ) data shown in Table 2 were obtained by monitoring the Eu^{3+} $^5D_0$ excited level and Tb^{3+} $^5D_3$ and $^5D_4$ levels. The obtained curves are shown in Fig. S7 and were best adjusted by applying a mono-exponential fit. The Tb^{3+} lifetime values were used to estimate the Tb→Eu ET efficiency by applying Eq. (6) [38], where τ_1 is the lifetime value for the codoped sample and τ_{10} is the lifetime value for the Tb^{3+} single doped samples. The emission spectra for the single doped Ba_2SiO_4:Tb^{3+} (2%, 1%, 0.5% and 0.1%-doped) are shown in Fig. S7 and the ET efficiencies are shown in Table 2.

$$\eta_{Tb\rightarrow Eu} = 1-\frac{\tau_1}{\tau_{10}} \tag{6}$$

From Table 2, the Tb→Eu ET efficiency increase in the samples that have Eu^{3+} content much lower or higher than that of Tb^{3+}, showing that the Tb→Eu ET prevails in relation to the opposite process. In these cases, the ET efficiency value from the Tb^{3+} $^5D_3$ level is higher than that from the $^5D_4$ one, showing that the Tb→Eu ET occurs mainly via the Tb^{3+} $^5D_3$ level. As expected from the emission spectra, when the Tb^{3+} content is much lower than that of Eu^{3+} (Tb(0.5)Eu(4) and Tb (0.1)Eu(4)), the ET efficiency from both $^5D_3$ and $^5D_4$ levels are 100%, indicating that this is the best condition to improve the Eu^{3+} efficiency. This efficient Tb→Eu ET can also be evidenced by the increase of the Eu^{3+} $^5D_0$ lifetime values for these samples when compared to the single doped Ba_2SiO_4:Eu^{3+} (compare in Table 1 the lifetime values for the samples single-doped or codoped with 4% of Eu^{3+}).

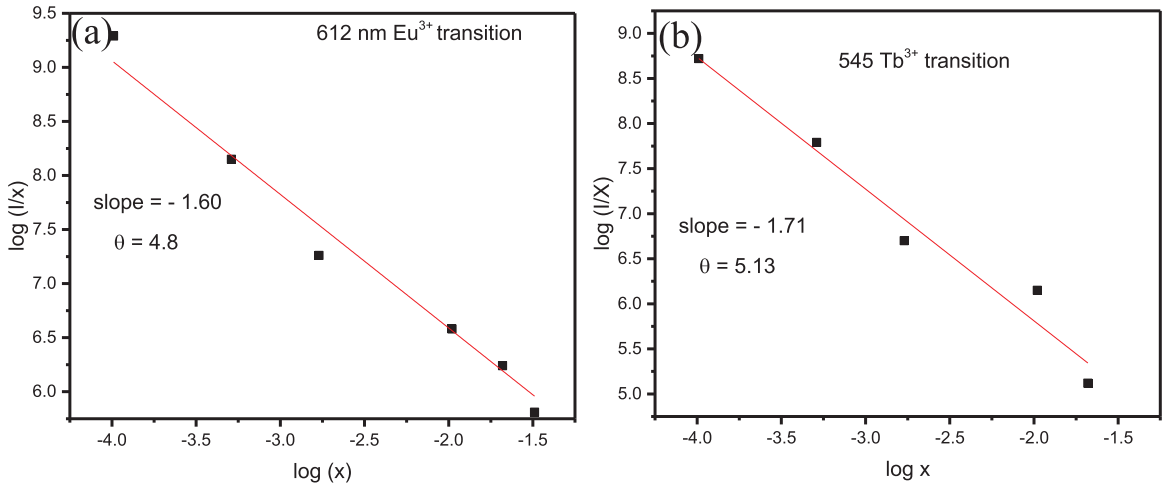

Fig. 5. Linear fitting of log(x) versus log(I/x) for Ba_2SiO_4:Eu^{3+}(x%),Tb^{3+}(1%) phosphors considering the emission intensity at (a) 612 nm and (b) 545 nm.

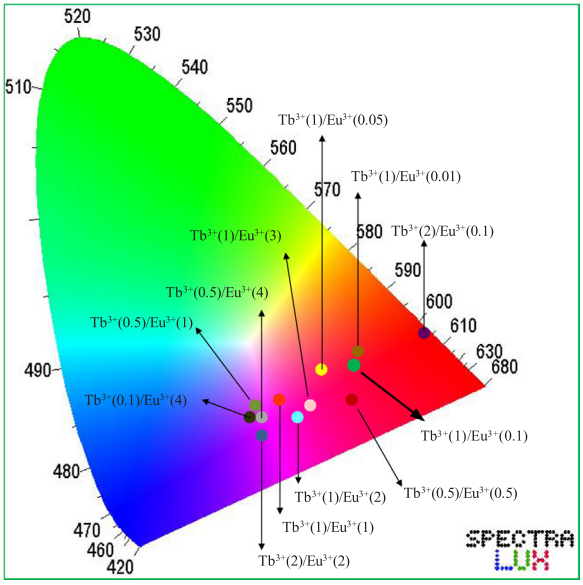

Fig. 6. CIE chromaticity diagram for the Tb^{3+} and Eu^{3+}-codoped Ba_2SiO_4 obtained from Spectra Lux software [31], and the emission spectra collected under 250 nm excitation measured at room temperature.

When the Eu^{3+} and Tb^{3+} contents are similar (samples doped with Tb(1)Eu(1), Tb(0.5)Eu(0.5), Tb(2)Eu(2) and Tb(0.5)Eu(1)), the Tb→Eu ET efficiency for the $^5D_3$ level is lower than that of the others, and the ET efficiency from the $^5D_4$ level is higher than 100% or very low. These results show that in the $^5D_3$ level, the Eu→Tb ET is more efficient for the $^5D_3$ level population in relation to the other samples, and as consequence, decrease the Tb→Eu ET efficiency. Yet considering the $^5D_4$ level, a Tb→Eu ET efficiency higher than 100% indicates that the opposite process is the main ET process, contributing to the population of the $^5D_4$ level and its lifetime value increase. Also, in some cases, a low $^5D_4$ Tb→Eu ET efficiency is an indicative that the opposite ET process is dominating. In this context, the Eu→Tb ET occurs mainly via the $^5D_4$ level.

The Eu^{3+} $^5D_0$ lifetime values were used to estimate the Eu^{3+} quantum efficiency (η_{Eu}) also shown in Table 2. The quantum efficiency is the greatness that correlate the radiative (A_{rad}) and the non-radiative (A_{nrad}) contributions from an emitting level (Eq. (7)) [32].

$$\eta = \frac{A_{rad}}{A_{rad} + A_{nrad}} \tag{7}$$

The A_{rad} contributions are calculated by the main radiative contributions related to the $^5D_0 \rightarrow {}^7F_1$ Eu^{3+} transitions, as shown in Eq. (8) [32]. Yet, the A_{nrad} values are determined directly from the lifetime values, as represented in Eq. (9) [32].

$$A_{rad} = \sum^{J} A_{0-j} \tag{8}$$

$$A_{total} = \frac{1}{\tau} = A_{rad} + A_{nrad} \tag{9}$$

For samples doped with 1% of Tb^{3+}, the η_{Eu} decrease when the Eu^{3+} concentration increase up to 2%, from then on, the η_{Eu} has an increment. The reduction of η_{Eu} is due to the $Eu^{3+} \rightarrow Tb^{3+}$ ET that overcomes the opposite process in these samples, as previously discussed, decreasing the population of Eu^{3+} $^5D_0$ level. However, as the $Eu^{3+} \rightarrow Tb^{3+}$ ET is not efficient at high Eu^{3+} doping concentration, the $Tb^{3+} \rightarrow Eu^{3+}$ ET is the dominant process and, as consequence, increase the population of the Eu^{3+} $^5D_0$ level. A similar profile is observed for samples doped with 0.5% of Tb^{3+}.

The Tb^{3+} ions are acting as sensitizer for the Eu^{3+} ions in some specific conditions. Recently, we reported the η_{Eu} for the Eu^{3+} 4%-doped sample as 68.2%, as shown in Table 2 [13]. However, when we doped this sample with 0.5% or 0.1% of Tb^{3+}, the η_{Eu} increase to 77.9% and 88.9%, respectively, enhancing in 20% the Eu^{3+} quantum efficiency. This occurs because the $Tb^{3+} \rightarrow Eu^{3+}$ ET is high and the Tb^{3+} ions act as sensitizers to the Eu^{3+} ions, increasing the $^5D_0$ level population and as consequence, enhances the Eu^{3+} radiative rate, and its quantum efficiency.

4. Conclusions

An energy transfer approach between Eu^{3+} and Tb^{3+} ions in monophasic Ba_2SiO_4 matrix successfully prepared by the sol–gel route was proposed. Both Eu^{3+} and Tb^{3+} emissions could be detected under 250 nm excitation, with an unexpected intense Tb^{3+} blue emission from the $^5D_3$ level at relatively high Tb^{3+} concentration. However, at relatively high Eu^{3+} concentrations, the Tb^{3+} emission was quenched. It was possible to tune the phosphor emission from red to pink by varying the Eu^{3+} and Tb^{3+} content. Considering all doping studied combinations, the energy transfer from Tb^{3+} to Eu^{3+} ions is taking place in all samples, but the inverse process only dominates when both Tb^{3+} and Eu^{3+} content are similar. The Tb→Eu ET occurs mainly from the Tb^{3+} $^5D_3$ level to the Eu^{3+} excited levels but the Eu→Tb ET occurs mainly from the Eu^{3+} excited levels to the Tb^{3+} $^5D_3$ one. Also, when the Eu^{3+} content is much higher than the Tb^{3+} concentration, the Eu^{3+} quantum efficiency increase, due to the $Tb^{3+} \rightarrow Eu^{3+}$ ET, showing that

Table 2
Tb→Eu ET efficiency for all codoped samples (the $\eta_{Tb\rightarrow Eu}$ ($^5D_3$) and the $\eta_{Tb\rightarrow Eu}$ ($^5D_4$) correspond to the ET from the Tb^{3+} $^5D_3$ and $^5D_4$ levels to the Eu^{3+} levels, respectively), Tb^{3+} $^5D_3$ (τ_{Tb} $^5D_3$) and $^5D_4$ (τ_{Tb} $^5D_4$) lifetime values, Eu^{3+} experimental Judd-Ofelt intensity parameters (Ω_2, Ω_4), Eu^{3+} $^5D_0$ lifetime values (τ_{Eu}), and Eu^{3+} quantum efficiency (η_{Eu}) for the prepared phosphors.

Tb/Eu (%)	$\eta_{Tb\rightarrow Eu}$ ($^5D_3$) / %	$\eta_{Tb\rightarrow Eu}$ ($^5D_4$) / %	τ_{Tb} $^5D_3$ /ms	τ_{Tb} $^5D_4$/ms	Ω_2 / pm	Ω_4 / pm	τ_{Eu} / ms	η_{Eu} / %
2/2	78	108	0.43	1.53	5.59	4.80	0.73	33.8
2/0.1	82	12	0.36	1.24	4.66	4.69	1.36	56.1
1/3	100[a]	100[a]	-[b]	-[b]	5.69	5.18	0.99	46.7
1/2	100[a]	100[a]	-[b]	-[b]	5.81	5.22	0.57	27.3
1/1	91	8	0.20	1.26	5.30	4.74	0.83	37.5
1/0.1	91	17	0.20	1.14	4.98	4.96	1.28	55.4
1/0.05	92	12	0.18	1.21	4.57	4.60	1.22	49.6
1/0.01	100	12	-[b]	1.22	4.65	4.90	1.49	61.1
0.5/4	100[a]	100[a]	-[b]	-[b]	5.90	4.57	1.67	77.9
0.5/1	90	136	0.27	1.80	5.11	4.40	1.26	54.4
0.5/0.5	84	114	0.43	1.51	5.25	3.90	1.37	58.7
0.1/4	100[a]	100[a]	-[b]	-[b]	5.74	4.25	1.97	88.9
0/4 [13]	–	–	–	–	6.20	6.10	1.34	68.2
0/3 [13]	–	–	–	–	6.20	7.20	1.29	58.8
0/2 [13]	–	–	–	–	6.40	5.60	1.11	55.6
0/1 [13]	–	–	–	–	5.90	5.90	1.33	66.5
2/0	–	–	1.92	1.41	–	–	–	–
1/0	–	–	2.21	1.37	–	–	–	–
0.5/0	–	–	2.71	1.32	–	–	–	–
0.1/0	–	–	3.33	1.31	–	–	–	–

[a] For the samples that do not have $^5D_3$ and $^5D_4$ lifetime values, the Tb→Eu ET efficiency was considered as 100%.
[b] Some samples do not shown Tb^{3+} emission and as consequence do not have lifetime values.

Tb^{3+} ions is acting as sensitizer to Eu^{3+} ions. Finally, the energy transfer between the doping ions is dominated by the dipole-dipole multipolar interactions.

Acknowledgements

The authors are thankful to the Brazilian agencies CNPq (307385/2015), CAPES, and FAPESP for the financial research support. Airton G. B. Junior is grateful to FAPESP for the award of some scholarships (Grant No.2012/13876-9, 2015/10394-1, and 2016/20421-9). The authors thank to Laboratório de Microscopia Eletrônica de Varredura (FCT-UNESP), research group in sol-gel (UNIFRAN), and Laboratório de compósitos e cerâmicas funcionais (FCT-UNESP).

Conflicts of interest

There are no conflicts to declare.

Appendix A. Supporting information

Supplementary data associated with this article can be found in the online version at doi:10.1016/j.jlumin.2018.03.057.

References

[1] G. Gasparotto, M.A. Cebim, M.S. Goes, S.A.M. Lima, M.R. Davolos, J.A. Varela, C.O. Paiva-Santos, M.A. Zaghete, Correlation between the spectroscopic and structural properties with the occupation of Eu^{3+} sites in powdered Eu^{3+}-doped $LiTaO_3$prepared by the Pechini method, J. Appl. Phys. 106 (2009) (063509-5.).
[2] L. Chen, C. Lin, C. Yeh, R. Liu, Light converting inorganic phosphors for white light-emitting diodes, Materials (3) (2010) 2172–2195.
[3] Z. Wang, S. Guo, Q. Li, X. Zhang, T. Li, P. Li, Z. Yang, Q. Guo, Luminescent properties of Ba_2SiO_4:Eu^{3+} for white light emitting diodes, Physica B (2013) 110–113.
[4] F. Steudel, S. Loos, B. Ahrens, S. Schweizer, Quantum efficiency and energy transfer processes in rare-earth doped borate glass for solid-state lighting, J. Lumin. 170 (2016) 770–777.
[5] H. Ji, L. Wang, M.S. Molokeev, N. Hirosaki, R. Xie, Z. Huang, Z. Xia, O.M. ten Kate, Li Liub, V.V. Atuchin, New garnet structure phosphors, $Lu_{3-x}Y_xMgAl_3SiO_{12}$:$Ce^{3+}$ (x = 0–3), developed by solid solution design, J. Mater. Chem. C. 4 (2016) 2359–2366.
[6] Koen Binnemans, Interpretation of europium(III) spectra, Coord. Chem. Rev. 295 (2015) 1–45.
[7] S.A.M. Lima, F.A. Sigoli, M.R. Davolos, M. Jafelicci Jr., Europium(III)-containing zinc oxide from Pechini method, J. Alloy. Compd. 344 (2002) 280–284.
[8] J.G. Bunzli, Lanthanide luminescence for biomedical analyses and imaging, Chem. Rev. 110 (2010) 2729–2755.
[9] S.V. Eliseeva, J.G. Bunzli, Lanthanide luminescence for functional materials and bio-sciences, Chem. Soc. Rev. 39 (2010) 189–227.
[10] A.A. Silva, M.A. Cebim, M.R. Davolos, Excitation mechanisms and effects of dopant concentration in Gd_2O_2S:Tb^{3+} phosphor, J. Lumin. 128 (2008) 1165–1168.
[11] A.M. Pires, M.R. Davolos, Luminescence of Europium(III) and Manganese(II) in barium and zinc orthosilicate, Chem. Mater. 13 (2001) 21–27.
[12] A.M. Pires, M.R. Davolos, O.L. Malta, Eu^{3+}-O^{2-}associates luminescence in Ba_2SiO_4, J. Lumin. 72 (1997) 244–246.
[13] A.G. Bispo-Jr, D.A. Ceccato, S.A.M. Lima, A.M. Pires, Red phosphor based on Eu^{3+}-isoelectronically doped Ba_2SiO_4 obtained via sol-gel route for solid state lightning, RSC Adv. 7 (2017) 53752–53762.
[14] F. Steudel, S. Loos, B. Ahrens, S. Schweizer, Quantum efficiency and energy transfer processes in rare-earth doped borate glass for solid-state lighting, J. Lumin. 170 (2016) 770–777.
[15] L. Zhou, B. Yan, Synthesis, microstructure and photoluminescence of Eu3 + /Tb3 + activated Y_2SiO_5 nanophosphors by new silicate sources, Appl. Surf. Sci. 254 (2008) 1847–1851.
[16] W. Guo, Y. Tian, P. Huang, L. Wang, Q. Shi, C. Cui, Color tunable luminescence in novel $Li_3Ba_2Y_3(WO_4)_8$:Tb^{3+}, Eu^{3+} phosphor for white LEDs, Ceram. Int. 42 (2016) 5427–5432.
[17] S. Som, S.K. Sharma, Eu^{3+}/Tb^{3+}-codoped Y_2O_3 nanophosphors: Rietveld refinement, bandgap and photoluminescence optimization, J. Phys. D: Appl. Phys. 45 (2012) 415102.
[18] A.J. Fernández-Carrión, M. Ocaña, J. García-Sevillano, E. Cantelar, A. Isabel Becerro, New single-phase, white-light-emitting phosphors based on δ-$Gd_2Si_2O_7$ for solid-state lighting, J. Phys. Chem. C 118 (2014) 18035–18043.
[19] M.A. Tshabalala, H.C. Swart, O.M. Ntwaeaborwa, TOF SIMS analysis and generation of white photoluminescence from strontium silicate codoped with europium and terbium, J. Vac. Sci. Technol. A 32 (2014) 021401–021406.
[20] P.A. Raymundo-Pereira, D.A. Ceccato, D., A.G.B. Junior, M.F.S. Teixeira, S.A.M. Lima, A.M. Pires, Study on the structural and electrocatalytic properties of Ba^{2+}- and Eu^{3+}-doped silica xerogelsas sensory platforms, RSC Adv. 6 (2016) 104529–104536.
[21] J.K. Han, M.E. Hannah, A. Piquette, J.B. Talbot, K.C. Mishra, J. McKittrick, Europium-activated $KSrPO_4$–$(Ba,Sr)_2SiO_4$ solid solutions as color-tunable phosphors for near-UV light-emitting diode applications, J. Am. Ceram. Soc. 96 (2013) 526–1532.
[22] A.L. Patterson, The scherrer formula for x-ray particle size determination, Phys. Rev. 56 (1939) 978–982.
[23] I. Couwenberg, K. Binnemans, H. De Leebeeck, C. Gorller-Walrand, Spectroscopic properties of the trivalent terbium ion in the huntite matrix $TbAl_3(BO_3)_4$, J. Alloy. Compd. 274 (1998) 157–163.
[24] W.T. Carnall, G.L. Goodman, K. Rajnak, R.S. Rana, A systematic analysis of the spectra of the lanthanides doped into single crystal LaF_3, J. Chem. Phys. 90 (1989) 3443–3457.
[25] Y. Fu, Y. Hu, A blue–green-emitting phosphor $Na_2Ca_3Si_2O_8$:Tb^{3+} with tunable emission color manipulated by cross-relaxation, J. Mater. Sci: Mater. Electron. 27 (2016) 3867–3872.
[26] J. Zhang, B. Chen, Z. Liang, X. Li, J. Sun, R. Zhong, L. Cheng, H. Zhong, Interionic cross relaxation and tunable color luminescence in KY_3F_{10}:Tb^{3+}nano/microcrystals

synthesized by hydrothermal approach, J. Fluor. Chem. 144 (2012) 1–6.
[27] N. Guo, C. Jia, J. Li, Y. Zhao, R. Ouyang, W. Lu, Color tuning and energy transfer in Eu^{2+}/Mn^{2+}-doped $Ba_3Y(PO_4)_3$eulytite-type orthophosphate phosphors, RSC Adv. 5 (2015) 46517–46524.
[28] O.L. Malta, Mechanisms of non-radiative energy transfer involving lanthanide ions revisited, J. Non-Cryst. Solids 354 (2008) 4770–4776.
[29] D.L. Dexter, J.H. Schulman, Theory of concentration quenching in inorganic phosphors, J. Chem. Phys. 22 (1954) 1063–1070.
[30] L.G. Uitert, Characterization of energy transfer interactions between rare earth ions, J. Electrochem. Soc. 14 (1967) 1048–1053.
[31] P.A. Santa-cruz, F.S. Teles, Spectra Lux Software. Versão 2.0 RENAMI, U. Federal de Pernambuco, 2003.
[32] G.F. de Saá, O.L. Malta, C. de Mello Donegaa, A.M. Simas, R.L. Longo, P.A. Santa-Cruz, E.F. da Silva Jr, Spectroscopic properties and design of highly luminescent lanthanide coordination complexes, Coord. Chem. Rev. 196 (2000) 165–195.
[33] A.P. Duarte, M. Gressier, M. Menu, J. Dexpert-Ghys, J.M.A. Caiut, S.J.L. Ribeiro, Structural and luminescence properties of silica-based hybrids containing new silylated-diketonato europium(III) complex, J. Chem. Phys. C 116 (2012) 505–515.
[34] T. Grzyb, S. Lis, Structural and spectroscopic properties of LaOF:Eu^{3+} nanocrystals prepared by the sol-gel pechini method, Inorg. Chem. 50 (2011) 8112–8120.
[35] A.M. Pires, M.R. Davolos, E.B. Stucchi, Eu as a spectroscopic probe in phosphors based on spherical fine particle gadolinium compounds, Int. J. Inorg. Mater. 3 (2001) 785–790.
[36] T. Grzyb, S. Lis, Structural and spectroscopic properties of LaOF:Eu^{3+} nanocrystals prepared by the sol–gel pechini method, Inorg.Chem 50 (2011), pp. 8112–8120.
[37] W.T. Carnall, Handbook on the Physics and Chemistry of Rare Earths 3 (1979), p. 171.
[38] P. Ghosh, A. Kar, A. Patra, Energy transfer study between Ce^{3+} and Tb^{3+} ions in doped and core-shell sodium yttrium fluoride nanocrystals, Nanoscale 2 (2010) 1196–1202.